batteries

MDPI

Article

Coupled Electro-Thermal-Aging Battery Pack Modeling—Part 1: Cell Level

Hadi Pasdarshahri [1], Émile Veilleux [1,*], William Mooney [1], Luc G. Fréchette [2], François Grondin [3] and David Rancourt [1]

[1] Createk Innovation Group, Interdisciplinary Institute for Technological Innovation (3IT), Université de Sherbrooke, Sherbrooke, QC J1K 0A5, Canada
[2] Calogy Solutions, 4445 Rue Robitaille, Sherbrooke, QC J1L 2Y9, Canada
[3] IntRoLab, Interdisciplinary Institute for Technological Innovation (3IT), Université de Sherbrooke, Sherbrooke, QC J1K 0A5, Canada
* Correspondence: emile.veilleux@usherbrooke.ca

Abstract: This paper presents a modeling approach to capture the coupled effects of electrical–thermal aging in Li-ion batteries at the cell level. The proposed semi-empirical method allows for a relatively high accuracy and low computational cost compared to expensive computer simulations. This is something current models often lack but is essential for system level simulations, relevant for electric vehicle manufacturers. The aging analysis includes both cycling and calendar effects across the lifetime of the cell and reversible and irreversible heat in a lumped-mass model to capture the temperature evolution of the cell in operation. The Thévenin equivalent circuit model with capacitance used to simulate the electrical behavior of the cell was experimentally validated, showing a high correlation with the proposed model during the charging and discharging phases. A maximum error of 3% on the voltage reading was identified during discharge with the complete model. This model was also designed to be used as a stepping stone for a comprehensive model at the module and vehicle levels that can later be used by designers.

Keywords: Li-ion batteries; semi-empirical model; aging; capacity fade

Citation: Pasdarshahri, H.; Veilleux, É.; Mooney, W.; Fréchette, L.G.; Grondin, F.; Rancourt, D. Coupled Electro-Thermal-Aging Battery Pack Modeling—Part 1: Cell Level. *Batteries* **2024**, *10*, 404. https://doi.org/10.3390/batteries10110404

Academic Editor: Pascal Venet

Received: 19 October 2024
Revised: 13 November 2024
Accepted: 15 November 2024
Published: 17 November 2024

1. Introduction

The global commitment to reduce carbon emissions has an impact on the transportation industry. The electrification of various types of vehicles is seen as a viable way forward and is currently benefiting from a high interest in technological development. This leads to new challenges in terms of energy storage, safety, and operation [1].

Battery pack level models are required for the design, management, and performance evaluation over the lifetime of electric vehicles [2]. Low-level models are generally fast (setup and code execution) and allow for preliminary analysis and overview, but cannot capture complex thermal paths or cell-to-cell and cell-to-pack interactions when scaled up to the vehicle level. On the other hand, high-fidelity models allow for specific detailed analysis but are very time consuming both in model setup (geometry definition, boundary conditions) and in the actual simulation. This leads to the need for a medium-fidelity battery pack model that can bridge the gap.

The sole use of physics-based models or data-driven models each present their own strengths and weaknesses when applied to battery modeling [1,3]. This is the case either because of parameter uncertainties or because of the large amount of experimental data required. Here, a semi-empirical model is proposed to achieve the desired medium-fidelity results.

There are two main types of aging to consider in battery modeling. These are (1) cycling, related to the use of the battery, and (2) calendar, related to its storage [4]. Modern approaches should consider both to ensure reliable results [5–7]. Battery aging involves

a decrease in capacity and an increase in internal resistance, also referred to as internal resistance growth (IRG) [8–10]. Both cycle aging and calendar aging irreversibly consume battery capacity through either a loss of lithium inventory (LLI) or a loss of active material (LAM) [11]. LLI refers to the reactions that affect the amount of lithium available to cycle between the anode and the cathode. Some of these reactions are the development of a solid electrolyte interface, lithium plating, and electrolyte decomposition [12]. LAM refers to mechanisms the lead to the reduction in available material for the electrochemical reactions, both for the anode and the cathode [13]. References [14,15] should be consulted for more information on aging mechanisms and how the operating conditions change the chemical reactions within a cell. To reduce the degradation of batteries in practical scenarios, several studies have focused on developing empirical models to find out the dominant mechanisms of overall aging as well as control strategies.

Collath et al. [16] reviewed strategies for managing battery degradation. This review identifies the relevant aging mechanisms and degradation modeling techniques and synthesizes the key findings in the field. These aging mechanisms can also be referred to as stress factors and usually affect the battery in a coupled manner [10]. Kucinskis et al. [17] analyzed the Arrhenius plots in the context of C-rate, cell aging, and electrode properties. For reference, C-rate is defined as the charge or discharge current divided by the capacity of the battery. C-rate is a commonly used metric because it allows comparison of different cells on a standardized scale. The studies showed that the crossover point between the dominant aging mechanisms, and therefore the optimal operating temperature for Li-ion cells, depends on factors such as C-rate, anode coating thickness/particle size, state of health, and the shape of the capacity fade curve. Recognizing and accounting for the shift in the dominant aging mechanism can aid in the design of battery systems with extended life. Typically, aging models are calibrated under constant storage or cycling conditions. In practice, storage and cycling conditions often vary. Karger et al. [18] offered various distinct approaches to modeling capacity degradation during dynamic operation. They discussed the potential of using these approaches in the cycling aging calculations. Jafari et al. [4] reviewed the various models used to study the degradation of Li-ion batteries, spanning different scales such as materials and application. Their review provides a summary of the key aging variables, analyzes the mathematical representations of the models, and discusses the advantages and disadvantages at each scale. The primary objective of this review is to consolidate methods and results across multiple technologies and form factors for the most common Li-ion battery technologies.

The use of data-driven models has become the preferred approach for estimating battery health and remaining useful life. Several semi-empirical models have been developed for Li-ion batteries depending on the chemistry and scenario used for both calendar and cycling aging [5,19–23]. Instead of relying on the complex modeling of internal chemical processes as functions of operating conditions, semi-empirical models directly link the aging with the operating conditions. Each of these models includes a temperature factor and at least one term related to voltage, state of charge (SOC), or anode potential. Regarding cycling aging, Baghdadi et al. [23] used temperature, depth of discharge (DOD), and current as stress factors. In contrast, the models of Schmalstieg et al. [19] ignored the effect of current or C-rate, which may limit their applicability, especially at higher C-rates. Wang et al. [21] used C-rate as a stress factor but omitted the DOD term, which is a common inclusion in other models. More recently, data-driven modeling also found favor in predicting battery life due to its remarkable accuracy, as highlighted in studies such as that of Severson et al. [24]. It is important to note, however, that both the quality and quantity of the training dataset are essential to this methodology. The absence of either can potentially have a significant impact on the accuracy and effectiveness of the model. Recently, Hosen et al. [3] introduced a novel approach by developing a neural network model. They extended their investigation by adapting their semi-empirical and data-driven models using a comprehensive self-generated dataset consisting of 40 lithium nickel man-

ganese cobalt (NMC) cells. Their study is the first to compare different performance-based models, all constructed from a single dataset.

Various electrothermal aging models have already been proposed in the literature using some of these aging estimation methods. Calearo et al. [25] proposed a modeling methodology focusing on the electrical, thermal, and aging dynamics of Li-ion batteries with the application in electric vehicles (EVs). The model inputs include only electrical power and ambient temperature, and its outputs are compared with actual measurements. Their model predicts the electrothermal behavior of the battery pack with errors less than 5% and estimates the capacity decrease within one percentage point of the battery management system (BMS) readings. Perez et al. [26] focused on developing a model to evaluate fast and safe charging protocols to improve battery practicality for mobile applications such as smartphones and electric vehicles. Their methodology optimally balances charge time and health degradation while adhering to electrical and thermal constraints. Saqli et al. [27] introduced an improved electrothermal battery model to develop a co-estimation scheme for battery capacity, SOC, and core and surface temperatures. They showed that regular updates of battery capacity improve the accuracy of SOC estimates and track battery health. Real-time updates of operating temperatures, capacity, and SOC were shown to significantly improve estimator accuracy. Han et al. [28] developed and verified six control-oriented battery electrothermal aging models with varying accuracies in terminal voltage and temperature simulations. Their study then quantitatively analyzes the impact of different battery models on the model predictive control-based energy management strategy, considering battery dynamics, computation time, and operating cost in a plug-in hybrid electric vehicle. Simulation results show that focusing on the early ages of battery use significantly improves speed and accuracy. Although these studies show an improvement in battery state prediction by adding aging to their model, the increase in resistance due to aging is not considered. This paper aims to balance these methods to allow for scaling up the model while maintaining sufficient accuracy and low computational complexity.

Because the electrical, thermal, and chemical responses of the cell are intricately related when simulating the complete behavior of a cell, it is critical to design models accordingly. This is especially the case when a scaling to the pack level is envisioned. However, few studies address the comprehensive evaluation of these coupled effects on cell responses [29]. Most studies ignore the resistance increase during aging, which has a significant impact on the prediction of the internal heat generation of the battery. On the other hand, battery aging is influenced by several thermophysical factors, including storage and cycling temperature, depth of discharge, C-rate, throughput, storage SOC, and storage time. Throughput is defined as the net energy delivered by the cell or battery over its lifetime [10]. The proposed model is designed to account for the interplay between electrical, thermal, and aging phenomena within a Li-ion cell, evaluating all of these aging stress factors. Since the proposed model includes the influence of the electrical and thermal characteristics of the cell on both calendar- and cycling-induced aging, it can explore the capacity degradation and increased resistance due to cell aging. These, in turn, provide valuable insights that feed back into the electrical and thermal models. The aging process is based on a comprehensive empirical model calibrated by accelerated aging experiments. Both individual aging models and the final integrated model have been validated against experimental data, ensuring their accuracy and reliability.

This paper presents the first building block of a complete battery pack model with a cell level analysis. The proposed approach is a comprehensive semi-empirical electrothermal aging (ETA) model for a typical Li-ion cell. This paper presents an overview of the model, the experimental methodology used to generate the required data, and the parameter extraction procedure used to complete the model.

2. Model Description

Although the electrical, thermal, and aging behaviors of a Li-ion cell are highly coupled, these can be presented as three separate models interacting with each other at each time

step as shown in Figure 1. The electrical model described in Section 2.1 is used to compute the instantaneous electrical properties of a cell subjected to a power or current load (user inputs), as a function of its state of charge, average temperature, and state of health (SOH). The temperature used to determine the electrical properties is an output of the thermal model described in Section 2.2. This model computes the cell temperature based on external heat transfer and by computing internal heat generation using the electrical properties from the electrical model at a given time. Boundary conditions of the thermal model include ambient temperature and heat transfer coefficient between the environment and the cell. The response of the electro-thermal model to an input power profile is solved numerically using implicit methods. The aging model, calibrated using data from aging tests for both calendar and cycling scenarios, is used to update the cell's capacity and internal resistance using results from both the electrical and thermal models. The time scale of aging processes is considerably greater than the electro-thermal response of the cell. Consequently, updates to the cell's electrical properties can be carried out with larger time steps than what is used for the electro-thermal model, as described in Section 2.3.

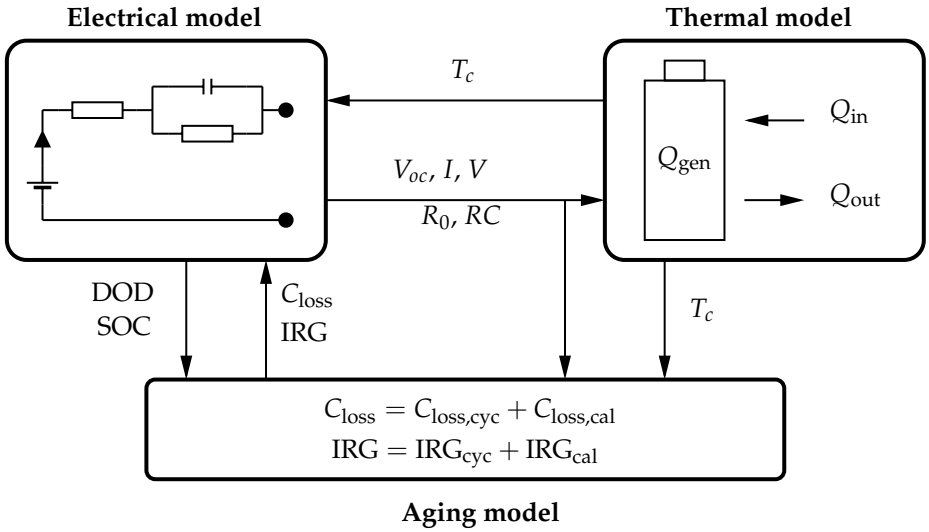

Figure 1. Cell-level electrothermal aging model.

2.1. Electrical Model

The equivalent circuit model (ECM) used in this study is a Thévenin model [30] with a single resistance–capacitance pair (1-RC), as shown in Figure 2. Equations (1)–(3) are used to compute the voltage (V) and the current (I) or power (P) of the cell at a given time:

$$V = V_{oc} - R_0 I - V_1 \tag{1}$$

$$\frac{dV_1}{dt} = \frac{I}{C_1} - \frac{V_1}{C_1 R_1} \tag{2}$$

$$P = VI \tag{3}$$

with the open circuit voltage (OCV) V_{oc} and the voltage of the RC pair V_1. Cell internal resistance (R_0), RC pair resistance (R_1) and capacitance (C_1), and OCV are all semi-empirical functions of the SOC and average cell temperature T_c. These parameters are extracted from standard hybrid power pulse characterization (HPPC) tests which are described in Section 3.1. The state of charge of a cell is expressed as the ratio of remaining capacity to its full capacity under specific operating conditions and is calculated using Coulomb counting:

$$\mathrm{SOC}(t) = \mathrm{SOC}(0) + \frac{1}{3600\, C(t)} \int_0^t I(t)dt \tag{4}$$

where t is the time in seconds and $C(t)$ is the rated capacity in A h. The capacity is a function of time because aging degradation mechanisms lead to a decrease in capacity over time.

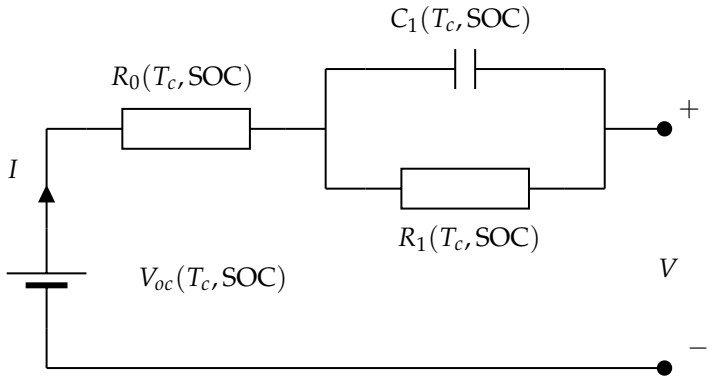

Figure 2. Equivalent circuit model of the cell.

2.2. Thermal Model

The temperature of a cell at a given time is calculated using (5), assuming a the cell can be modeled as a single thermal mass with internal heat generation and subject to uniform external heat transfer.

$$mc_p \frac{dT_c(t)}{dt} = Q_{gen} + (Q_{\text{in}} - Q_{\text{out}}) \tag{5}$$

where m and c_p are, respectively, the mass and the specific heat capacity of the cell and Q is the thermal power, generated, entering, or leaving the cell control volume. The internal heat generation of the cell (Q_{gen}) is calculated with (6), which splits Li-ion cell's heat generation in an irreversible term and a reversible term, the latter introducing the reversible heat coefficient $\frac{dV_{oc}}{dT}$:

$$Q_{gen} = I(V - V_{oc}) - IT_c \frac{dV_{oc}}{dT} \tag{6}$$

The irreversible heat, or Joule heating, is directly calculated using the output of the ECM. Reversible heat, also known as entropic heat, is associated with the reversible electrochemical processes taking place during charging and discharging of the Li-ion cell. These reactions result in the production or absorption of heat, expressed using the reversible heat coefficient. This coefficient was obtained using data from an industrial partner.

2.3. Aging Model

The aging model plays a pivotal role in the comprehensive generalized ETA model. This study incorporates both cycle and calendar aging. The methodology used for modeling capacity degradation closely aligns with the semi-empirical approach of an Arrhenius kinetic-based aging model. The following paragraphs provide a more detailed description of the aging model that is briefly described in a previous publication [31].

Studies on cell-level aging modeling have an empirical orientation and provide fitted mathematical models based on extensive experimental data. These data are generated through both accelerated and non-accelerated testing methods for various battery technologies [4].

For the cycle aging, an Arrhenius kinetic-based aging model is used. The capacity loss due to cycling can be modeled by a generic model proposed by Wang et al. [21]:

$$C_{\text{loss,cyc}} = B \exp\left(\frac{-E_{a,\text{cyc}} + \lambda \cdot \text{C-rate}}{\overline{R}T}\right) H^z \tag{7}$$

where T is the temperature of the cell during cycling, H is the charging throughput, $\overline{R}$ is the gas constant, and C-rate is the average cycling C-rate. E_a, B, λ, and z are parameters fitted

using experimental data. In (7), the effect of the DOD in cycle aging is neglected. To obtain a more comprehensive aging model, the acceleration term due to DOD effect [32] is added to (7) to result in (8)

$$C_{\text{loss,cyc}} = B \exp\left(\frac{-E_{a,\text{cyc}} + \lambda \cdot \text{C-rate}}{\overline{R}T}\right) H^z \left(\frac{\text{DOD}}{\text{DOD}_{\text{ref}}}\right)^{\alpha} \tag{8}$$

where α is another fitted parameter. The capacity loss in (8) is represented in percentage. Cycle aging is function of cell temperature, DOD, charge/discharge current, and the number of cycles. Internal resistance growth due to cycle aging is modeled using the same approach as for the capacity loss. Again, IRG is expressed as a percentage increase in the nominal internal resistance of the cell. The fitted parameters used for cycle IRG (9) are denoted by the subscript R to differentiate them from capacity loss fitted parameters:

$$\text{IRG}_{\text{cyc}} = B_R \exp\left(\frac{-E_{a,\text{cyc},R} + \lambda_R \cdot C_{rate}}{\overline{R}T}\right) H^{z_R} \left(\frac{\text{DOD}}{\text{DOD}_{\text{ref}}}\right)^{\alpha_R} \tag{9}$$

The model used for calendar aging is based on the work of Wilke et al. [33]. The capacity loss due to calendar aging is calculated using (10), which is a function of storage time (t) and two acceleration parameters:

$$C_{\text{loss,cal}} = k_{\text{cal},0} \theta_T \theta_V t^{n_{\text{cal}}} \tag{10}$$

with $k_{\text{cal},0}$ and n_{cal} being fitted parameters. The Arrhenius acceleration with temperature (θ_T) and the Tafel acceleration with voltage (θ_V) are derived by Wilke et al. [33]:

$$\theta_T = \exp\left[\frac{-E_{a,\text{cal}}}{\overline{R}}\left(\frac{1}{T} - \frac{1}{T_{\text{ref}}}\right)\right] \tag{11}$$

$$\theta_V = \exp\left[\frac{-a_1 F}{\overline{R}}\left(\frac{1 + a_2\text{SOC} + a_3\text{SOC}^2}{T} - \frac{1 + a_2\text{SOC}_{\text{ref}} + a_3\text{SOC}_{\text{ref}}^2}{T_{\text{ref}}}\right)\right] \tag{12}$$

where t is the storage time, F is Faraday's constant, and a_1, a_2, a_3 are fitted parameters. Equations (10)–(12) are also used for internal resistance growth due to calendar aging, with parameters fitted for IRG instead of capacity loss. The effects of calendar and cycle aging on remaining capacity and total internal resistance are assumed to be independent and additive, with C_{loss} and IRG in percentage:

$$C = C_{\text{initial}}\left(1 - 0.01\left(C_{\text{loss,cyc}} + C_{\text{loss,cal}}\right)\right) \tag{13}$$

$$R_0 = R_{0,\text{initial}}\left(1 + 0.01\left(\text{IRG}_{\text{cyc}} + \text{IRG}_{\text{cal}}\right)\right) \tag{14}$$

It is important to note that the initial cell capacity C_{initial} is not constrained to a specific value, allowing for potential break-in mechanisms that may result in temporary capacity increases [34]. The reference value for T_{ref}, DOD_{ref}, and SOC_{ref} are set at 25 °C, 0.5, and 0.5, respectively [32].

3. Experimental Method

This section covers the experimental work and data reduction process used to create the semi-empirical ETA model. The cells used in this work are NMC 18650 Li-ions, with a nominal capacity of 3.2 A h and a nominal voltage of 3.60 V. The cells and test equipment used are sourced by the industrial partner.

3.1. Electro-Thermal Model Tests

To characterize the cell's ECM parameters, HPPC [35], charge, discharge, and OCV tests were conducted. The OCV test followed the methodology outlined in [36,37]. Prior to

initiating the cell test, a full charge of the cell was ensured. Subsequently, the cell underwent a slow discharge (C/20) to a minimum operating voltage, with continuous monitoring of cell voltage and accumulated ampere-hours discharged. Following the discharge, the cell was charged (at C/20) to a maximum operating voltage, with continuous monitoring of cell voltage and accumulated ampere-hours charged. All tests were conducted at temperatures of 15 °C, 25 °C, and 35 °C, mapping typical operating conditions. To maintain the temperature constant during a set of tests, the cells were placed in climate chambers and immersed in a dielectric fluid. The climate chamber provides heat when required. Cooling is achieved by circulating a coolant in a tubular coil also immersed in the dielectric fluid and connected to a table top chiller (15L PolyScience Refrigerated Circulator). The charge and discharge of the cells are realized using a Chroma-17216M-10-6 battery tester.

3.2. Aging Model Tests

The aging model was built using both experimental data and parameters from the literature. The capacity loss due to calendar aging uses parameters taken directly from Wilke et al. [33]. For the internal resistance growth due to calendar aging, raw test data were obtained from an industrial partner. Test conditions of the data points that were used for calendar aging IRG parameters are shown in Table 1. Cycle aging parameters were obtained experimentally using intermittent discharge and HPPC tests for 15 °C, 25 °C, and 35 °C. The experimental setup described in Section 3.1 was used. The cycling test procedure for the 8 cells used for cycling tests is as follows:

1. Initialization: The test cells are placed in environmental chambers for two hours to establish the target temperature.
2. Charge: The cells undergo charging through a constant current (CC) step, reaching a cut-off voltage of 4.2 V (dependent on DOD). This is followed by a constant voltage (CV) step at 4.2 V (dependent on DOD) until the charge current drops below 50 mA.
3. Pause: A 10 min rest period between the charge and discharge phases.
4. Discharge: The cells undergo discharge at a constant current until the 2.5 V cut-off voltage is reached.
5. Pause: A 10 min rest period precedes the initialization of the subsequent cycle.
6. Steps 2 to 5 are repeated over a span of 3–4 weeks.
7. Reference tests: All aging tests are intermittently interrupted every 3–4 weeks to perform a reference performance test (RPT) and resistance measurement.

Table 1. Calendar aging test conditions.

Test Number	**1**	**2**	**3**	**4**	**5**	**6**	**7**	**8**	**9**	**10**	**11**	**12**
Temperature, °C	55	35	45	45	25	35	25	25	45	55	25	35
Average state of charge (SOC), %	50	50	50	80	50	80	80	95	95	80	100	100

RPTs are used to gather data used for the aging model. During a RPT, a cell is placed in a climate chamber at 25 °C for two hours to ensure stabilization of the ionic carriers. It is then fully charged following a CCCV pattern with a 0.5 C constant current (CC) phase and a maximum cell voltage of 4.2 V for the constant voltage (CV) phase. Charge stops when the current reaches 4% of the available cell capacity or 50 mA. After the charge, a 15 min rest period at 25 °C is used. Subsequently, the battery cell is fully discharged by applying a 0.2 C discharge rate. Discharge stops when the cut-off voltage of 2.5 V is reached.

Cycling test parameters are presented in Table 2 and the experimental capacity fade and internal resistance increase are shown in Figure 3. The capacity and resistance of the cell exhibit sensitivity to temperature, DOD, and C-rate. As expected, higher C-rates lead to increase in capacity fade. The cells cycled at 40 °C show more capacity fade than the cells cycled at 25 °C, with the exception of Cell Number 6 (80% DOD, 1.9 C discharge, 25 °C). This discrepancy in the behavior makes the aging characterization difficult.

Table 2. Cycle aging test conditions *.

Test Number	1	2	3	4	5	6	7	8
Temperature, °C	40	40	40	40	25	25	25	25
Depth of discharge, %	80	80	40	40	80	80	40	40
Discharge C-rate, 1/h	1.0	1.9	1.0	1.9	1.0	1.9	1.0	1.9

* Charge C-rate of 0.9 C for all cycling tests.

Internal resistance of the cell is an important factor in heat generation calculations. Based on test results (see Figure 3b), the resistance shows an increase of up to 1.9 times its initial value. The trend in resistance increase indicates that DOD has a significant impact on the aging of the cells (Test Number 1, 2, 5, 6). The rate of resistance increases in considerably higher for test with 40 °C and 80% of DOD after 1000 A h of throughput.

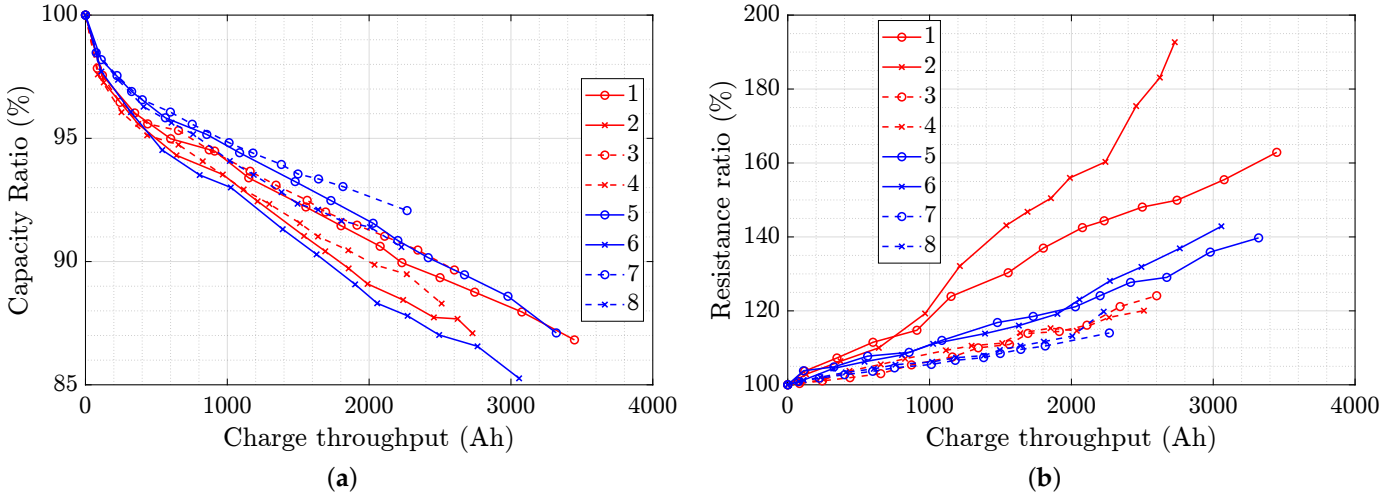

Figure 3. Cycle aging experimental results for Tests 1 through 8: (**a**) capacity and (**b**) resistance ratio.

The aging model is valid when used within the experimental test limits, and a wider dataset in terms of operating temperatures and SOC could extend the overall range of the model. The overall framework of this model would remain unchanged if a different aging dataset was used. This dataset is also limited in size, and the effect of values such as those of Cell Number 6 have a significant influence on the overall results.

4. Results and Discussion

4.1. Equivalent Circuit Model Parameters

The equivalent circuit model parameters presented in Table 3 were obtained using a nonlinear least square methods on OCV test results and HPPC test data. Note that at 90% SOC, the parameters of the RC pair are of a different order of magnitude than for the other SOCs. Although the physical meaning of these values is unclear, it is not affecting the precision of the model. To validate the ECM, a dynamic discharge drive profile was used and the predicted voltage response was compared with the experimental voltage measurements. Starting at 100% SOC, the cell was initially at rest for 900 s before starting the drive cycle discharge. The maximum discharge rate was 1.9 C, which is due to some of the battery tester's safety limitations. The results presented in Figure 4 aligns well with experimental results across the entire spectrum of discharge C-rates, validating the ECM.

Table 3. Equivalent circuit model parameters.

SOC, %	V_{oc}, V			R_0, Ω			R_1, Ω			C_1, F		
	15 °C	25 °C	35 °C	15 °C	25 °C	35 °C	15 °C	25 °C	35 °C	15 °C	25 °C	35 °C
10	3.37	3.32	3.38	0.1126	0.0623	0.0438	0.1289	0.0857	0.0407	461.6	321.4	1043.8
20	3.49	3.47	3.49	0.0656	0.0473	0.0451	0.0551	0.0239	0.0257	3142.0	2775.6	5886.4
30	3.52	3.53	3.56	0.0420	0.0397	0.0327	0.0464	0.0246	0.0342	493.0	1207.8	642.0
40	3.58	3.60	3.62	0.0512	0.0424	0.0397	0.0279	0.0257	0.0261	3459.9	2214.9	3558.1
50	3.66	3.67	3.68	0.0436	0.0413	0.0362	0.0343	0.0254	0.0226	1280.1	1959.4	1955.8
60	3.78	3.78	3.79	0.0477	0.0401	0.0372	0.0378	0.0253	0.0232	1639.8	1538.7	2163.0
70	3.86	3.87	3.87	0.0473	0.0414	0.0362	0.0297	0.0204	0.0161	1752.1	2192.3	2575.7
80	3.97	3.98	3.99	0.0477	0.0411	0.0372	0.0341	0.0297	0.0269	1266.0	1822.8	1898.1
90	4.03	4.07	4.07	0.0531	0.0471	0.0432	0.0099	0.0139	0.0094	13,422.0	6160.1	13,234.0
100	4.17	4.17	4.17	0.0585	0.0472	0.0390	0.0295	0.0292	0.0250	956.3	1225.6	1170.0

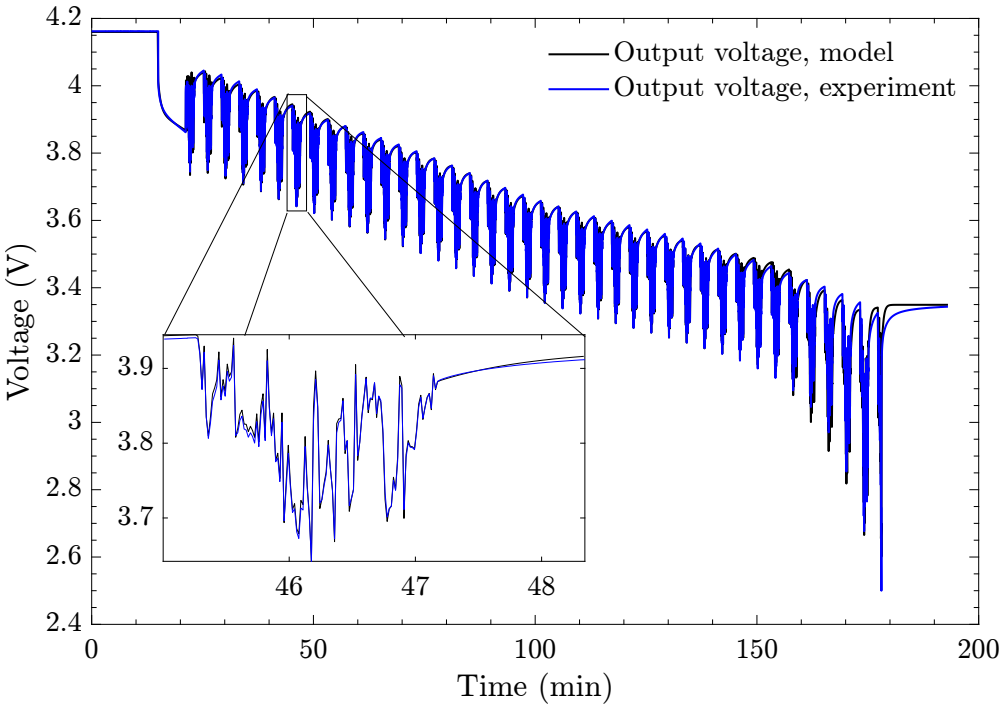

Figure 4. Validation of the cell characterization at 25 °C using a drive cycle.

4.2. Aging Model Parameters

Parametrization of the aging model was achieved using measured capacity and resistance values. The fitting process used a least-squares technique for model calibration where outliers in measurements or abnormal cell performance were excluded. To avoid local minima in the fitting procedure, a step-by-step and gradual adjustment of coefficients was employed. The acceleration factors for DOD and temperature were computed separately for Equations (8) and (10) (and their equivalent for IRG) and their dominant parameter's derivative. The complete model was fitted using initial guess for these acceleration factors. This approach reduces the number of iterations required while maintaining model accuracy. For model validation and to avoid overfitting, two experimental datasets were randomly selected and withheld from the calibration dataset. The calibration process was repeated multiple times with random experiments, and the semi-empirical model parameters were set when R^2 values over 0.95 were attained. The calibrated values for cycle aging, pertaining to both capacity and resistance estimation, are summarized in Table 4. The calibrated parameters of the calendar aging for capacity are from [33].

Table 4. Calibrated parameters for the semi-empirical aging model * (data from [31]).

Cycle Aging	**Capacity Fade**	**Internal Resistance Growth**
z	0.5750	1.1351
B	0.3239	4.6815
λ	481.85	1060
$E_{a,\mathrm{cyc}}$	33,040	37,800
α	0.1765	1.4564
Calendar Aging	**Capacity Fade [33]**	**Internal Resistance Growth**
n_{cal}	0.6562	0.9020
$k_{\mathrm{cal},0}$	0.02986	0.03042
$E_{a,\mathrm{cal}}$	54,054	53,889
a_1	0.0054	−0.1814
a_2	6.5858	0.6996
a_3	−3.2929	−0.6079

* The subscript R (see (9) example) is used for the calibrated parameters of the internal resistance growth models.

Figure 5 illustrates the validation of the resistance prediction for the calendar aging model. As depicted in the figure, the model accurately estimates cell resistance attributed to calendar aging, with prediction error below 10%. This level of accuracy underscores the effectiveness of the model in predicting resistance changes due to calendar aging.

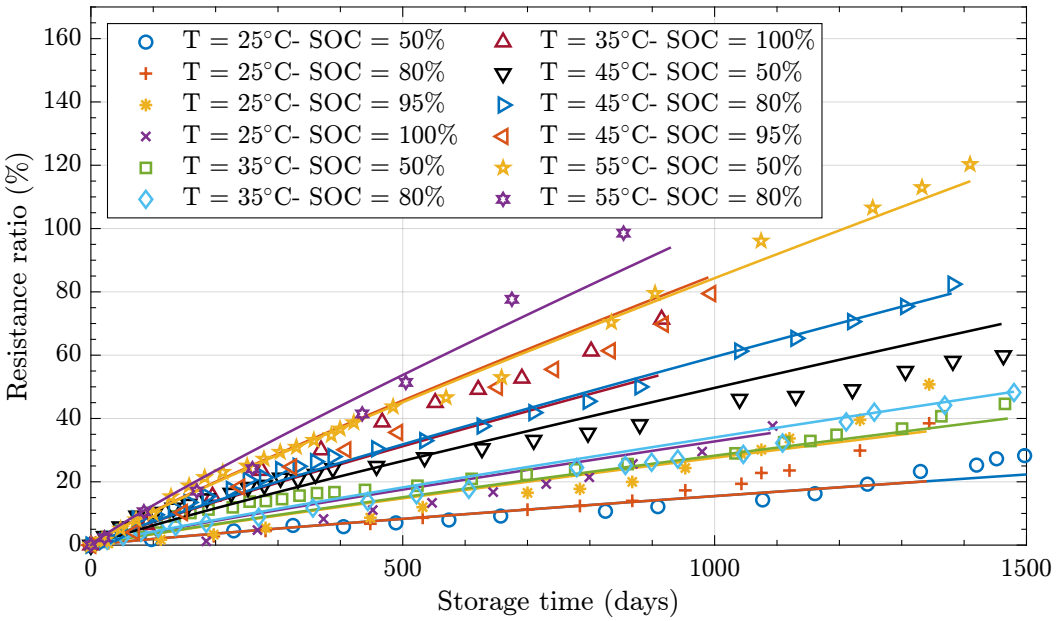

Figure 5. Validation of the aging model for resistance (calendar aging).

Figure 6 illustrates the validation of the cycle aging model, encompassing both capacity and resistance. The model predictions demonstrate a strong alignment with experimental results, validating the calibrated parameters. The resistance increase's response to cycle aging exhibits a non-linear trend in relation to charging throughput while being influenced by factors such as depth of discharge and temperature.

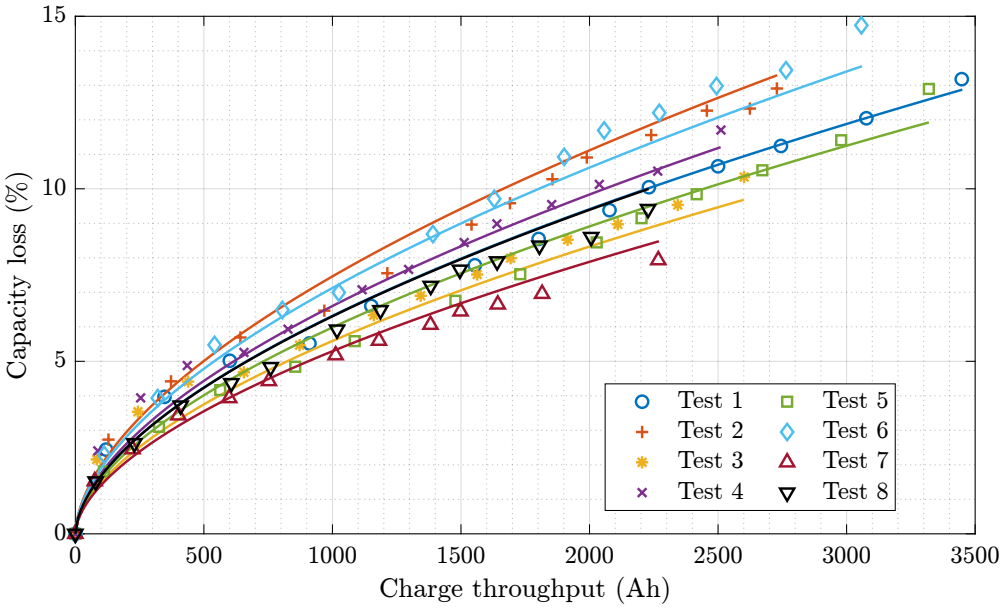

(**a**)

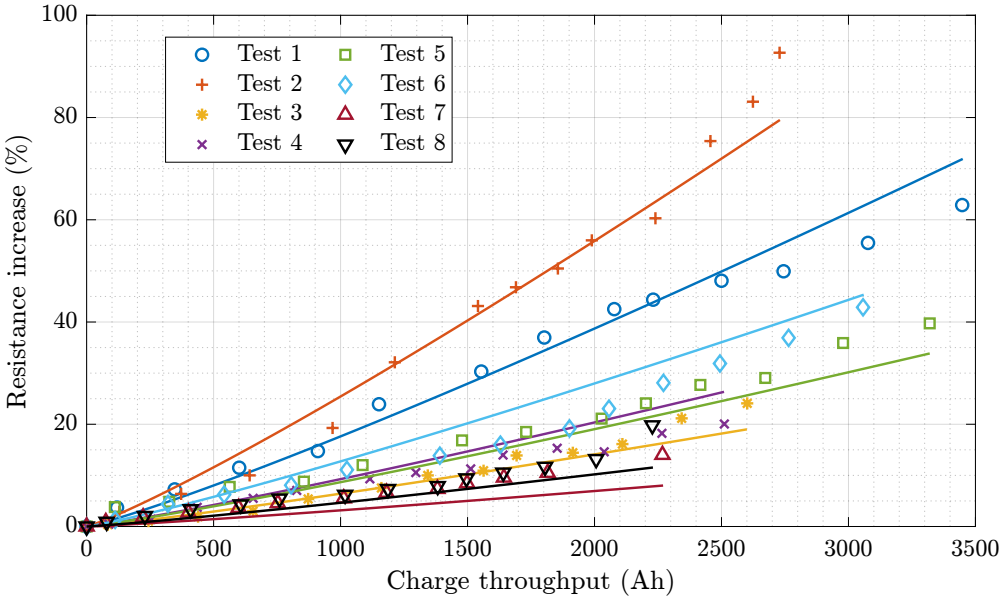

(**b**)

Figure 6. Validation of the cycle aging model for capacity and resistance: (**a**) capacity loss and (**b**) resistance increase.

4.3. Coupled Electro-Thermal Aging Model

The primary objective of this study is to present a comprehensive cell-level coupled electrical–thermal-aging model. A significant advantage of this model is its ability to predict cell voltage based on the cell's duty cycle. To validate the voltage prediction of the complete model, distinct experimental data from cycling at 25 °C, a depth of discharge (DOD) of 60%, a charging C-rate of 0.33, and a discharge C-rate of 1.0 were used. The findings are depicted in Figure 7 for various cycles. The proposed modeling and simulation approach yield highly accurate voltage predictions, particularly within the charging phase. The maximum error at the discharge phase is less than 3%. For a single cell, simulating thousands of cycles takes seconds, but the advantage of the semi-empirical approach is seen at a larger scale, when dozens of cells interact with each other in a battery pack.

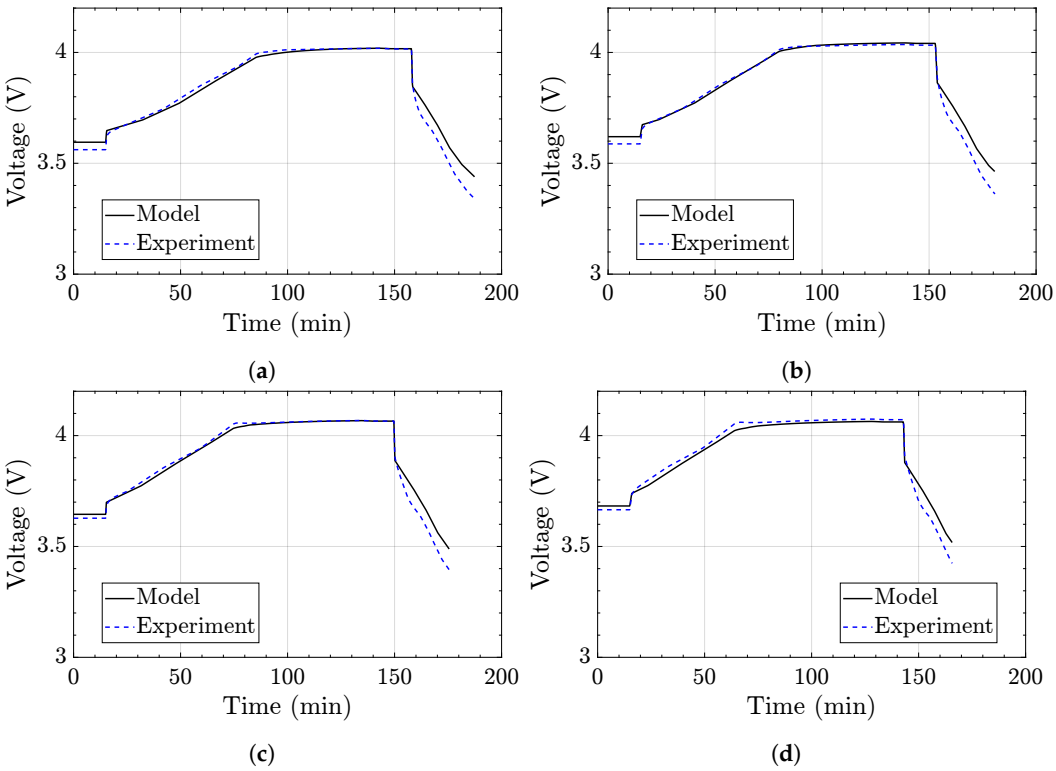

Figure 7. Validation of the coupled model: (**a**) 500 cycles (initial SOC: 30%), (**b**) 1000 cycles (initial SOC: 35%), (**c**) 1500 cycles (initial SOC: 40%), and (**d**) 2500 cycles (initial SOC: 45%).

5. Conclusions

A comprehensive semi-empirical Li-ion electrothermal aging model is developed and experimentally validated. The electrical model is based on the well-established Thévenin equivalent circuit model, for which the electrical parameters are extracted from tests at various temperatures and state of charge. The aging model considers both cycle and calendar aging using multiple key stress factors identified as such in the literature. Cycle aging considers C-rate, throughput, depth of discharge, and temperature, whereas calendar aging considers state of charge, temperature, and storage duration. In addition to this extensive list of stress factors, the model also considers instantaneous heat generation and cell electrical performance, something that, to the best of the authors' knowledge, is not present in the literature. The model undergoes rigorous calibration and validation using experimental data, accounting for both capacity degradation and internal resistance growth. The lumped-mass thermal model can be used to link the cell with its thermal management system. Combined with the aging model, this approach can be used to evaluate the capacity of a battery thermal management system to remove the heat generated as the internal resistance increases over time. The main drawback of this approach is the significant experimental effort required to generate the data to model a cell, highlighting the benefits of sharing model parameters as new cells and chemistries are characterized.

The next part of this research is aimed at the integration of this cell model to a module electro-thermal-aging model (METAM) battery module model, where dozens of cells are wired in series and parallel. Shifting from the cell-focused models, this METAM will also feature a multi-node thermal model that includes the main components of a battery module, notably its thermal management system and various thermal paths.

Author Contributions: Conceptualization, H.P. and L.G.F.; methodology, H.P.; software, H.P.; validation, H.P., É.V. and W.M.; formal analysis, H.P.; investigation, H.P.; resources, D.R.; data curation, H.P.; writing—original draft preparation, É.V. and W.M.; writing—review and editing, L.G.F., F.G. and D.R.; visualization, É.V.; supervision, project administration, funding acquisition, D.R. All authors have read and agreed to the published version of the manuscript.

Funding: This research and APC was funded by NSERC grant number ALLRP 560762-20 and CRIAQ (iNORTH).

Data Availability Statement: Dataset available on request from the authors.

Acknowledgments: The authors acknowledge the valuable contributions of Nicolas Voeltzel to the experimental work presented in this paper.

Conflicts of Interest: The authors declare no conflicts of interest. The funders had no role in the design of the study; analyses, or interpretation of data; in the writing of the manuscript; or in the decision to publish the results. Luc G. Fréchette is working at Calogy Solutions, a company that participated in the CRIAQ funding package used for this research. The content of this paper was not influenced by the participation of Calogy Solutions in research activities.

Abbreviations

The following abbreviations are used in this manuscript:

CCCV	Constant current, constant voltage
DOD	Depth of discharge
ECM	Equivalent circuit model
ETA	Electro-thermal aging
HPPC	Hybrid power pulse characterization
IRG	Internal resistance growth
LAM	Loss of active material
Li-ion	Lithium-ion
LLI	Loss of lithium inventory
OCV	Open circuit voltage
RPT	Reference performance test
SOC	State of charge
SOH	State of health

References

1. Zheng, Y.; Che, Y.; Hu, X.; Sui, X.; Stroe, D.I.; Teodorescu, R. Thermal state monitoring of lithium-ion batteries: Progress, challenges, and opportunities. *Prog. Energy Combust. Sci.* **2024**, *100*, 101120. [CrossRef]
2. Lucaferri, V.; Quercio, M.; Laudani, A.; Fulginei, F.R. A Review on Battery Model-Based and Data-Driven Methods for Battery Management Systems. *Energies* **2023**, *16*, 7807. [CrossRef]
3. Hosen, M.S.; Jaguemont, J.; van Mierlo, J.; Berecibar, M. Battery lifetime prediction and performance assessment of different modeling approaches. *iScience* **2021**, *24*, 102060. [CrossRef] [PubMed]
4. Jafari, M.; Khan, K.; Gauchia, L. Deterministic models of Li-ion battery aging: It is a matter of scale. *J. Energy Storage* **2018**, *20*, 67–77. [CrossRef]
5. Barcellona, S.; Colnago, S.; Dotelli, G.; Latorrata, S.; Piegari, L. Aging effect on the variation of Li-ion battery resistance as function of temperature and state of charge. *J. Energy Storage* **2022**, *50*, 104658. [CrossRef]
6. Krupp, A.; Beckmann, R.; Diekmann, T.; Ferg, E.; Schuldt, F.; Agert, C. Calendar aging model for lithium-ion batteries considering the influence of cell characterization. *J. Energy Storage* **2022**, *45*, 103506. [CrossRef]
7. Atalay, S.; Sheikh, M.; Mariani, A.; Merla, Y.; Bower, E.; Widanage, W.D. Theory of battery ageing in a lithium-ion battery: Capacity fade, nonlinear ageing and lifetime prediction. *J. Power Sources* **2020**, *478*, 229026. [CrossRef]
8. Wikner, E. Lithium ion Battery Aging: Battery Lifetime Testing and Physics-Based Modeling for Electric Vehicle Applications. Master's Thesis, Chalmers University of Technology, Göteborg, Sweden, 2017.
9. Attia, P.M.; Bills, A.; Planella, F.B.; Dechent, P.; dos Reis, G.; Dubarry, M.; Gasper, P.; Gilchrist, R.; Greenbank, S.; Howey, D.; et al. Review—"Knees" in Lithium-Ion Battery Aging Trajectories. *J. Electrochem. Soc.* **2022**, *169*, 060517. [CrossRef]
10. Vermeer, W.; Chandra-Mouli, G.R.; Bauer, P. A Comprehensive Review on the Characteristics and Modeling of Lithium-Ion Battery Aging. *IEEE Trans. Transp. Electrif.* **2022**, *8*, 2205–2232. [CrossRef]
11. Barré, A.; Deguilhem, B.; Grolleau, S.; Gérard, M.; Suard, F.; Riu, D. A review on lithium-ion battery ageing mechanisms and estimations for automotive applications. *J. Power Sources* **2013**, *241*, 680–689. [CrossRef]
12. Roy, P.; Shahjalal, M.; Shams, T.; Fly, A.; Stoyanov, S.; Ahsan, M.; Haider, J. A Critical Review on Battery Aging and State Estimation Technologies of Lithium-Ion Batteries: Prospects and Issues. *Electronics* **2023**, *12*, 4105. [CrossRef]
13. Ali, M.; Da Silva, C.; Amon, C. Multiscale Modelling Methodologies of Lithium-Ion Battery Aging: A Review of Most Recent Developments. *Batteries* **2023**, *9*, 434. [CrossRef]
14. Guo, J.; Li, Y.; Pedersen, K.; Stroe, D.-I. Lithium-Ion Battery Operation, Degradation, and Aging Mechanism in Electric Vehicles: An Overview. *Energies* **2021**, *14*, 5220. [CrossRef]

15. Xiao, Y.; Wen, J.; Yao, L.; Zheng, J.; Fang, Z.; Shen, Y. A comprehensive review of the lithium-ion battery state of health prognosis methods combining aging mechanism analysis. *J. Energy Storage* **2023**, *65*, 107347. [CrossRef]
16. Collath, N.; Tepe, B.; Englberger, S.; Jossen, A.; Hesse, H. Aging aware operation of lithium-ion battery energy storage systems: A review. *J. Energy Storage* **2022**, *55 Pt C*, 105634. [CrossRef]
17. Kucinskis, G.; Bozorgchenani, M.; Feinauer, M.; Kasper, M.; Wohlfahrt-Mehrens, M.; Waldmann, T. Arrhenius plots for Li-ion battery ageing as a function of temperature, C-rate, and ageing state—An experimental study. *J. Power Sources* **2022**, *549*, 232129. [CrossRef]
18. Karger, A.; Wildfeuer, L.; Aygül, D.; Maheshwari, A.; Singer, J.P.; Jossen, A. Modeling capacity fade of lithium-ion batteries during dynamic cycling considering path dependence. *J. Energy Storage* **2022**, *52 Pt A*, 104718. [CrossRef]
19. Schmalstieg, J.; Käbitz, S.; Ecker, M.; Sauer, D.U. A holistic aging model for Li(NiMnCo)O_2 based 18650 lithium-ion batteries. *J. Power Sources* **2014**, *257*, 325–334. [CrossRef]
20. Gasper, P.; Gering, K.; Dufek, E.; Smith, K. Challenging Practices of Algebraic Battery Life Models through Statistical Validation and Model Identification via Machine-Learning. *J. Electrochem. Soc.* **2021**, *168*, 020502. [CrossRef]
21. Wang, J.; Liu, P.; Hicks-Garner, J.; Sherman, E.; Soukiazian, S.; Verbrugge, M.; Tataria, H.; Musser, J.; Finamore, P. Cycle-life model for graphite-LiFePO_4 cells. *J. Power Sources* **2011**, *196*, 3942–3948. [CrossRef]
22. Nájera, J.; Arribas, J.R.; de Castro, R.M.; Núñez, C.S. Semi-empirical ageing model for LFP and NMC Li-ion battery chemistries. *J. Energy Storage* **2023**, *72 Pt A*, 108016. [CrossRef]
23. Baghdadi, I.; Briat, O.; Delatage, J.Y.; Vinassa, J.M.; Gyan, P. Dynamic Battery Aging Model: Representation of Reversible Capacity Losses Using First Order Model Approach. In Proceedings of the 2015 IEEE Vehicle Power and Propulsion Conference (VPPC), Montreal, QC, Canada, 19–22 October 2015; pp. 1–4. [CrossRef]
24. Severson, K.A.; Attia, P.M.; Jin, N.; Perkins, N.; Jiang, B.; Yang, Z.; Chen, M.H.; Aykol, M.; Herring, P.K.; Fraggedakis, D.; et al. Data-driven prediction of battery cycle life before capacity degradation. *Nat. Energy* **2019**, *4*, 383–391. [CrossRef]
25. Calearo, L.; Thingvad, A.; Ziras, C.; Marinelli, M. A methodology to model and validate electro-thermal-aging dynamics of electric vehicle battery packs. *J. Energy Storage* **2022**, *55 Pt B*, 105538. [CrossRef]
26. Perez, H.E.; Hu, X.; Dey, S.; Moura, S.J. Optimal Charging of Li-Ion Batteries with Coupled Electro-Thermal-Aging Dynamics. *IEEE Trans. Veh. Technol.* **2017**, *66*, 7761–7770. [CrossRef]
27. Saqli, K.; Bouchareb, H.; M'sirdi, N.K.; Bentaie, M.O. Lithium-ion battery electro-thermal modelling and internal states co-estimation for electric vehicles. *J. Energy Storage* **2023**, *63*, 107072. [CrossRef]
28. Han, J.; Liu, W.; Zheng, Y.; Khalatbarisoltani, A.; Yang, Y.; Hu, X. Health-conscious predictive energy management strategy with hybrid speed predictor for plug-in hybrid electric vehicles: Investigating the impact of battery electro-thermal-aging models. *Appl. Energy* **2023**, *352*, 121986. [CrossRef]
29. Petit, M.; Prada, E.; Sauvant-Moynot, V. Development of an empirical aging model for Li-ion batteries and application to assess the impact of Vehicle-to-Grid strategies on battery lifetime. *Appl. Energy* **2016**, *172*, 398–407. [CrossRef]
30. Nikolian, A.; Jaguemont, J.; de Hoog, J.; Goutam, S.; Omar, N.; van Den Bossche, P.; van Mierlo, J. Complete cell-level lithium-ion electrical ECM model for different chemistries (NMC, LFP, LTO) and temperatures (−5 °C to 45 °C)—Optimized modelling techniques. *Int. J. Electr. Power Energy Syst.* **2018**, *98*, 133–146. [CrossRef]
31. Veilleux, É.; Pasdarshahri, H.; Rancourt, D.; Daoudji, D. Passive Thermal Management of an Electric Trainer Aircraft Battery Pack Considering Aging. *J. Aircr.* 2025, *accepted*.
32. Santhanagopalan, S.; Smith, K.; Neubauer, J.; Kim, G.H.; Keyser, M.; Pesaran, A. *Design and Analysis of Large Lithium-Ion Battery Systems*, 1st ed.; Artech: London, UK, 2015.
33. Wilke, S.; Schweitzer, B.; Khateeb, S.; Al-Hallaj, S. Semi-Empirical Modeling of Capacity Fade: A Practical Approach for Battery Pack Manufacturers. *ECS Trans.* **2016**, *73*, 109–119. [CrossRef]
34. Smith, K.; Saxon, A.; Keyser, M.; Lundstrom, B.; Cao, Z.; Roc, A. Life prediction model for grid-connected Li-ion battery energy storage system. In Proceedings of the 2017 American Control Conference (ACC), Seattle, WA, USA, 24–26 May 2017; pp. 4062–4068. [CrossRef]
35. Nacu, R.C.; Fodorean, D. Lithium-Ion Cell Characterization, Using Hybrid Current Pulses, for Subsequent Battery Simulation in Mobility Applications. *Processes* **2022**, *10*, 2108. [CrossRef]
36. Plett, G. *Battery Management Systems,Volume I: Battery Modeling*; Artech: London, UK, 2015.
37. Plett, G. *Battery Management Systems, Volume II: Equivalent-Circuit Methods*; Artech: London, UK, 2015.